ULTRASONIC CHARACTERIZATION OF HORIZONTAL DENSITY VARIATIONS IN ORIENTED STRANDBOARD[1]

Ronnie Y. Vun†

Graduate Research Assistant

Qinglin Wu†

Associate Professor
School of Renewable Natural Resources
Louisiana State University Agricultural Center
Baton Rouge, LA 70803

and

Charles J. Monlezun

Associate Professor
Department of Experimental Statistics
Louisiana State University
Baton Rouge, LA 70803

(Received July 2002)

ABSTRACT

Random flake deposition in mat forming of oriented strandboard (OSB) results in inherent horizontal density variation that affects the panel strength quality. In this paper, a silicon gel coupled ultrasonic transmission (UT) was used to locate, map, and validate the horizontal density distribution in laboratory-made OSB. Two test boards were manufactured at each of three nominal density (ND) and three resin content (RC) levels. The UT variables velocity, attenuation, and root mean square voltage formed excellent complementary predictors of density for all RC and panel types. Based on the allowable ±10% variation in the average measured densities, both the general and polynomial models provided improved density prediction for boards at higher RC and ND levels. Using the contour and out-of-limits plots, the predicted horizontal densities gave a reasonable spatial approximation to the measured densities. All 6% RC panels with densities of 0.60 g/cm^3 or greater conformed well to the limits, with declining conformity towards the lower RC panels.

Keywords: Attenuation, horizontal density, OSB, velocity, quality control, ultrasonic.

INTRODUCTION

Strength properties of wood-based composites are related to mean panel density and the density distribution (both in-plane and across-panel thickness). In-plane or horizontal density variation in flakeboards is due to the presence of voids in the low density range and discrete consolidated particle structure in the high density range, created from the random particle deposition in the mat forming process (Suchsland 1962; Suchsland and Xu 1989; Vun et al. 2003). Process and raw material attributes, including strand type and geometry, amount of fines, and strand dimension and configuration, are the main factors contributing to the density variation. In-plane density variation contributes to crack formation and propagation during creep rupture of oriented strandboard (OSB), as noted by Vun and Beall (2002). The critical crack was initiated from the weakest point of the lowest density zones in the boards. The fracture was seen to propagate and follow the valleys of low density

[1] This paper (NO: 02-40-0456) is published with the approval of the Director of the Louisiana Agricultural Experiment Station.

† Member SWST.

zones. The magnitude of density variation, therefore, determines the creep resistance properties of OSB.

The European EN300 standard for panel manufacturing requires the horizontal density distribution in a panel to be within ±10% variation of the average panel density (Kruse et al. 2000). Modeling for the spatial structure of wood composites respective to processing and performance characteristics has been done using theoretical models and also by gravimetric destructive methods (Lu and Lam 2001; Oudjehane and Lam 1998; Steiner and Dai 1993). There is, however, lack of nondestructive techniques for determining the level of in-plane density variation in wood composites.

Nondestructive evaluation technologies have been utilized to study internal material properties such as defects and bonding quality for composite materials (Beall 2002; Bucur et al. 1998). The available techniques include forced vibration (Suddarth 1965), impact stress wave (Ross and Pellerin 1988; Vogt 1986), acousto-ultrasonics (Chen and Beall 2000), and acoustic emission (Vun and Beall 2002). Among these techniques, ultrasonic transmission (UT) is a test that involves transmission of ultrasonic pulses through a specimen and capture of the material response signatures (Jeong and Hsu 1995). Energy absorption and scatter of elastic waves due to discontinuities in interfacial boundaries result in an attenuated signal, characterizing internal structure and material properties (Judd and Wright 1978). The advantage of being able to scan a relatively large test area makes UT technique a safe and appropriate tool for studying the spatial variation of various material properties.

In an earlier study (Vun et al. 2003), direct-contact and non-contact techniques were applied to relate structural properties of OSB to such UT variables as velocity and attenuation. It was shown that the attenuation and root mean square (RMS) voltage variables are suitable as density predictors if the panel flake alignment level is not known; otherwise, the velocity could be used. A ''no-void'' densification point of OSB was identified by ultrasonic characterization. This no-void density is a transition point between the diminishing effect of incorporation of macrovoids at low density and the increasing plastic-strain hardening flow in the interfaces at high density ranges. The existence of reasonably good correlations among the UT parameters and the structural properties of OSB is an avenue for nondestructively predicting and examining spatial properties of the board.

In this paper, horizontal density distributions in OSB were obtained using a direct-contact UT technique. Individual density values were also measured on the respective scanning areas. The objectives were (1) to establish relationships between the UT variables and resin content (RC)/nominal density (ND) combinations; (2) to develop models for predicting UT variables from measured density; (3) to develop calibration models for predicting measured density from the UT variables; (4) to compare predicted values from various models to the control limits obtained using the EN300 standard; and (5) to map and compare the spatial distribution of predicted and measured density.

This paper discusses the descriptive statistics of the variables and their relationships to the RC and ND levels, the UT variable regressions on the average density (AD), the density prediction models, and the validation of the predicted to measured AD by percent out-of-limits and spatial graphics. Recommendations for future research are also discussed.

EXPERIMENTAL PROCEDURES

Specimen preparation

Loblolly pine trees of about 46 cm in diameter were harvested from the Lee Memorial Forest in south Louisiana. The logs were band-sawn into boards, which were flaked using a disc flaker to produce 76-mm-long flakes. The flakes were dried and screened. Eighteen random single-layer (560 × 510 × 13 mm) OSB panels were manufactured using liquid phenol formaldehyde resin. Each board

was made with 0.5% wax at one of three resin contents (either 2%, 4%, or 6%) and one of three nominal densities (either 0.4, 0.6, or 0.8 g/cm^3); two replicates of each board were made. The mats were hot-pressed for 7 min at 190°C under 4.44 MPa to cure the resin. After pressing, the boards were cooled at ambient conditions and then trimmed to reduce edge effects on test specimens. Each panel was conditioned at 24°C and 60% relative humidity to reach equilibrium. A 10 × 9 grid was then drawn on each board (Fig. 1b). Ninety individual specimens were obtained from the grid and were UT-measured. Each specimen was then sawn into 51 × 51 × 13 mm for the AD measurement.

Direct-contact transmission

UT measurements were taken in a through-transmission mode with two Panametrics 100-kHz transducers attached to opposite surfaces of the specimens (coupled using silicon gel) under a constant pressure of 3-kg weight. A Panametrics 5058 Pulser/Receiver was used to generate a 400-volt impulse that excited the transmitting transducer; the receiving transducer captured the transmitted signal (Fig. 1a). With a consistent setting of 40–60 dB gain or 0–80 dB attenuator, the signal was 30 dB preamplified, sampled at 5 MHz, digitized using a GageScope 8-bit CS225 card, and signal-processed. Velocity, impedance, attenuation, and RMS voltage of the ultrasound variables were used to characterize the properties of the OSB (Vun et al. 2003). The through-thickness velocity, V (m/s), is calculated as

$$V = d/t \tag{1}$$

where d is the sample thickness (mm) and t is the signal transit time (μs) across the thickness. The impedance of the material determines the alternating current of stress waves that flow through the material. As an analogy to a given alternating current potential difference, the impedance of the ultrasonic current is affected by difference in sample density. The material impedance, Z(Gg/s.m^2), is calculated as

$$Z = V \cdot \rho \tag{2}$$

where ρ is the sample density (10^{-3} kg/m^3). Attenuation is the energy loss associated with a decrease in the wave amplitude scattered by discontinuity and absorption among the different densities. Attenuation, α(dB), is given by

$$\alpha = 20 \text{ Log}(A/A_{ref}) \tag{3}$$

where A is the peak amplitude (v), and A_{ref} is the maximum amplitude allowable by the system (i.e., 5.2 v). The RMS voltage represents the signal intensity of the acquired signal, which is measured on a linear scale in voltage and computed by time-averaging rectification as

$$\text{RMS} = \left(\frac{1}{\Delta t} \int v^2(t)\, dt \right)^{1/2} \tag{4}$$

where Δt is the time interval (μs) and v is the voltage (v).

For each board, the basic direct contact UT measurements velocity (km/s), attenuation (−dB), and RMS voltage were taken for each of the ninety specimens defined by the grid. From these three variables and AD, five other measurements were also obtained: impedance, attenuation corrected to thickness (AT), attenuation corrected to thickness and density (ATD), RMS voltage corrected to thickness (RT), and RMS voltage corrected to thickness and density (RTD). The basic UT measurements were taken prior to ripping each board into ninety separate specimens.

Density profile

After UT testing, the panels were ripped to obtain separate 51 × 51 × 13-mm specimens. Density profiles across thickness and width for each specimen were obtained using a Quintek X-ray Density Profiler (QDP-01X). For each panel, the maximum, average, and minimum densities for each of the ninety test specimens were determined.

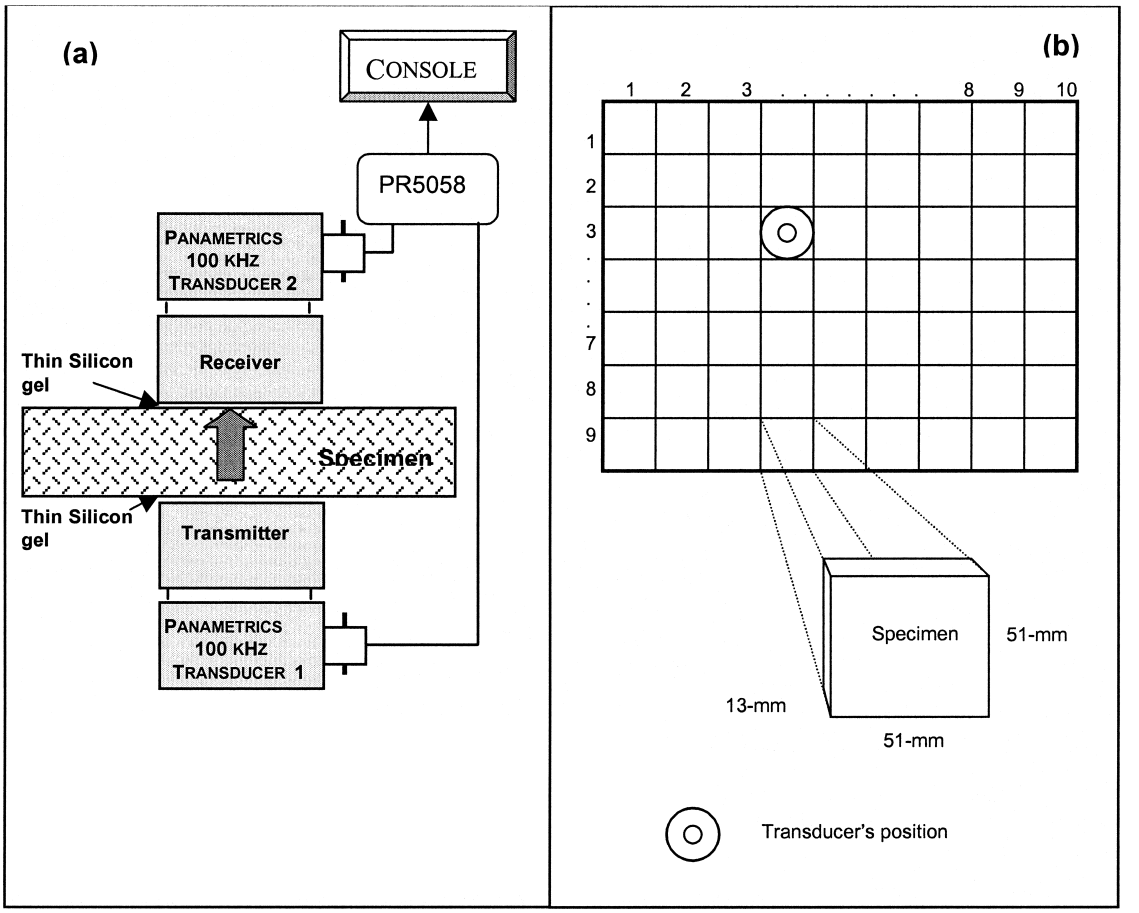

FIG. 1. Experimental setup for contact ultrasonic system (a) and test boards configuration (b).

Data

One of the two boards created at each RC/ND combination was randomly selected, giving a total of nine boards. The AD and UT measurements used in all of the analyses came from the $90 \cdot 9 = 810$ specimens obtained from the nine boards that were selected.

RESULTS AND DISCUSSION

Average density and UT properties

In this section, we shall examine the descriptive statistics of panel and UT properties segregated by the nine RC/ND combinations (see Tables 1 and 2). The coefficient of variation, or CV (defined as the sample standard deviation of the group divided by the average for the group, in percent) was calculated for each variable in these tables. For the variable AD, CV's decreased as ND levels increased for each RC level. This pattern of decreasing CV values as ND levels increased for each RC level was also observed for the UT variables velocity, impedance, and RMS voltage. The CV values for attenuation did not follow this pattern.

For each RC level, the vertical density profiles for the six specimens exhibited the typical M-shape of Fig. 2 (two profiles of each nominal density were chosen to exhibit the variability within the nominal density, and also to demonstrate the basic nature of the profiles for that nominal density). The high-density panels tended to have a sharper density contrast be-

TABLE 1. *Average values of the specimen mean densities and ultrasonic measurements.*

Basin content (%)	Nominal density (g/cm^3)	Average density (g/cm^3)	Ultrasonic variables				
			Z ($Gg/s{\cdot}m^2$)	ATD ($dB{\cdot}cm^3/mm{\cdot}g$)	RTD ($v{\cdot}cm^3/mm{\cdot}g$)	AT (dB/mm)	RT (v/mm)
2%	0.40	0.476	0.331	3.288	0.046	1.552	0.022
		(8)	(23)	(37)	(77)	(36)	(79)
	0.60	0.686	0.642	1.298	0.063 a	0.890	0.043
		(7)	(17)	(40)	(40)	(40)	(41)
	80	0.894	0.879	0.419	0.069 a	0.371	0.062
		(4)	(12)	(68)	(24)	(66)	(25)
4%	0.40	0.483	0.427	2.516	0.068	1.237	0.025
		(7)	(48)	(30)	(167)	(26)	(69)
	0.60	0.691	0.810	0.463	0.080 b	0.313	0.056
		(7)	(15)	(68)	(34)	(65)	(36)
	0.80	0.887	1.008	0.184	0.086 b	0.165	0.065
		(5)	(12)	(61)	(88)	(58)	(24)
6%	0.40	0.479	0.450	1.910	0.053	0.900	0.026
		(9)	(35)	(42)	(65)	(41)	(69)
	0.60	0.699	0.995	0.347	0.084	0.237	0.059 c
		(5)	(10)	(76)	(24)	(71)	(26)
	0.80	0.899	0.922	0.124	0.069	0.110	0.063 c
		(4)	(7)	(76)	(20)	(73)	(22)

For each RC level, reject Ho: $\mu_{.4} = \mu_{.6} = \mu_{.8}$ ($p < 0.01$ for $F(2, 267)$ for each UT variable.
a, b, c = p-value >0.12 not significantly different by $F(1, 267)$ test.
( ) = Coefficient of variation (CV%) of 90 specimens within a board, rounded to nearest integer.
Z = Acoustic impedance ($Gg./s{\cdot}m^2$).
AT = Attenuation coefficient (dB/mm) corrected for thickness.
RT = RMS coefficient (v/mm) corrected for thickness.
ATD = Attenuation coefficient ($dB{\cdot}cm^3/mm{\cdot}g$) corrected for density and thickness.
RTD = RMS coefficient ($v{\cdot}cm^3/mm{\cdot}g$) corrected for density and thickness.

tween face and core layers, since high-density elements at the surface decreased more rapidly following the exponential decreasing rate of differential heat transfer towards the core (also observed by Smith 1982). The low-density panels had smaller differential heat transfer from the surface to core during hot pressing, leading to a less pronounced dip and rise in the density profile. The conspicuous high-face and low-core density layers can also be attributed to the elevated low-density areas in orthogonal flake boundaries (Lenth and Kamke 1996), causing physical hindrance to heat transfer necessarily for resin curing.

The existence of a larger density fluctuation in the density profile for the low-density specimens led to higher attenuation, lower velocity, and lower RMS voltage values. This is consistent with the finding that the high attenuation and dispersion of the ultrasonic energy was caused by discontinuities arising from interfacial flakes in the low-density core for wood composites (Chen and Beall 2000). In addition, the impedance (Z) increased with nominal density in the 2% and 4% RC's but peaked and decreased slightly in the 6% RC panels (Table 1). The maximum value of impedance of 1.008 $Gg/s.m^2$ occurred at RC 4% in combination with ND 0.8. Note the similar trend for the variables RTD and RT. For each RC level, the variables RT and RTD increased with increasing average density, the lone exception being the RTD at 6% RC. However, the variables ATD and AT consistently decreased with increasing density for each RC (in a greater magnitude for the low-density panels).

Two-factor UT ANOVA models

With RC and ND as the factors, a two-factor analysis of variance, having 801 error degrees of freedom, was performed on each of the basic UT variables in Table 2. All RC and ND

TABLE 2. *Comparisons of resin content and nominal density to ultrasonic measurements.*

Resin content %	Nominal density (g/cm^3)	LSMean	CV(%)	P-VALUE*						
Velocity (km/s)										
2	0.4	0.693	(21)	2; 0.4	<.0001	<.0001	<.0001		<.0001		
	0.6	0.936	(16)		2; 0.6	0.0342		<.0001		<.0001	
	0.8	0.985	(12)			2; 0.8			<.0001		0.0731
4	0.4	0.830	(30)	2%//4%	0.4	***	4; 0.4	<.0001	<.0001	<.0001	
	0.6	1.169	(12)		0.0032	0.6		4; 0.6	0.5597		<.0001
	0.8	1.156	(19)			0.0561	0.8		4; 0.8		<.0001
6	0.4	0.924	(29)	2%	**			0.4	**	6; 0.4	<.0001	<.0001
	0.6	1.422	(8)	0.0014	4%			<.0001	0.6		6; 0.6	<.0001
	0.8	1.026	(7)	<.0001	<.0001	6%		<.0001	<.0001	0.8		6; 0.8
Attenuation (−dB)												
2	0.4	19.19	(36)	2; 0.4	<.0001	<.0001	<.0001			<.0001		
	0.6	10.83	(41)		2; 0.6	<.0001		<.0001			<.0001	
	0.8	4.49	(66)			2; 0.8			<.0001			<.0001
4	0.4	14.86	(29)				4; 0.4	<.0001	<.0001	<.0001		
	0.6	3.78	(65)					4; 0.6	0.0013		0.0816	
	0.8	2.02	(61)						4; 0.8			0.2341
6	0.4	10.79	(41)	2%	**			0.4	**	6; 0.4	<.0001	<.0001
	0.6	2.83	(72)	<.0001	4%			<.0001	0.6		6; 0.6	0.0077
	0.8	1.36	(72)	<.0001	<.0001	6%		<.0001	<.0001	0.8		6; 0.8
RMS-Voltage (v)												
2	0.4	0.272	(79)	2; 0.4	<.0001	<.0001	0.2783			0.1900		
	0.6	0.528	(41)		2; 0.6	<.0001		<.0001			<.0001	
	0.8	0.754	(25)			2; 0.8			0.1927			0.4609
4	0.4	0.305	(72)				4; 0.4	<.0001	<.0001	0.8207		
	0.6	0.672	(36)					4; 0.6	<.0001		0.3254	
	0.8	0.794	(30)						4; 0.8			0.5716
6	0.4	0.312	(69)	2%	**			0.4	**	6; 0.4	<.0001	<.0001
	0.6	0.702	(26)	0.0165	4%			0.0043	0.6		6; 0.6	0.0149
	0.8	0.77	(22)	0.0007	0.5486	6%		0.8457	0.0017	0.8		6; 0.8

( ) = Coefficient of variation (CV%) of 90 specimens within a board, rounded to nearest integer.
* p-values for pairwise comparisons of the RC [ND] at each ND [RC] level using a two-factor analysis of variance with 801 error degrees of freedom.
** p-values for pairwise F(2, 801) tests for parallel RC curves and parallel ND curves, respectively.
*** F(1, 801) test for part of RC 2% and 4% parallel.

main effects were highly significant ($p < 0.0001$) for each UT variable, as were all RC*ND interactions ($p < 0.0001$), except for the variable RMS voltage ($p = 0.0031$). Graphical evidence of these findings appears in Figs. 3a and 3b, in which the group averages of Table 2 are plotted versus the ND (RC) levels by the RC (ND) levels, respectively.

Although the three RMS voltage curves of Fig. 3a are not parallel (due to significant RC*ND interaction), the 4% and 6% RC curves are parallel ($p = 0.5486$ from Table 2). In addition, the RMS voltage ND 0.4 and 0.8 curves of Fig. 3b are parallel ($p = 0.8457$). Although the entire velocity RC 2% and 4% curves are marginally not parallel ($p = 0.0114$), the portion of these two curves between ND 0.6 and 0.8 curves is marginally parallel ($p = 0.0561$). All attenuation curves for all RC and ND levels are not parallel ($p < 0.0001$).

Results of the pairwise comparisons of the three RC (ND) levels at each ND (RC) level for all UT variables appear in Table 2. For the UT variable velocity, the pairwise comparisons of the three ND levels for each RC level

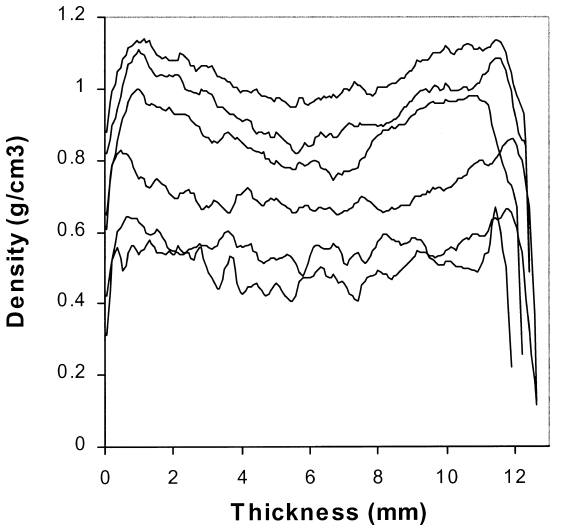

FIG. 2. Measured vertical density specimen profiles (Two typical specimen profiles per nominal density—same basic shapes for all RC's).

were highly significant, with two exceptions: for RC 4%, there is no difference between ND 0.6 and 0.8 ($p = 0.5597$); for RC 2%, there is only marginal evidence of a difference between ND 0.6 and 0.8 ($p = 0.0342$). Again, for velocity, the pairwise comparisons of the three RC levels for each ND level were highly significant, except for RC 2% and 6% at ND 0.8 ($p = 0.0731$).

For the UT variable attenuation, all pairwise comparisons of the ND levels at each RC were highly significant; while the pairwise comparisons of the RC levels at each ND were highly significant, except for RC levels 4% and 6% at ND 0.6 and, again, at ND 0.8 ($p = 0.0816$ and $p = 0.2341$, respectively). As for the UT variable RMS voltage, all of the pairwise comparisons of the three ND levels for each RC level were highly significant, the lone exception being the marginal significance ($p = 0.0149$) of ND 0.6 versus ND 0.8 for RC 6% level. However, all of the pairwise comparisons of the three RC levels for each ND level were not significantly different, with two exceptions: for ND 0.6, RC 2% is highly significantly different from both 4% and 6% ($p < 0.0001$).

UT regressions on average density

Scatter plots of the UT measurements versus AD in Fig. 4 reveal a quadratic relationship for each RC (as was the case in an earlier study on aspen OSB by Vun et al. 2003). Accordingly, a simultaneous regression model with $810 - 9 = 801$ degrees of freedom for error, allowing different least squares quadratic functions for the three RC's, was fit to each UT variable. For each UT variable, all three quadratic coefficients were highly significant ($p < 0.0001$), and the quadratic curves were found not to be parallel ($p < 0.0001$). Thus, inherently different quadratics are required to describe the relationship of each UT variable to AD at the three RC's (Table 3). The three inherently different least squares quadratic curves from the simultaneous regression model are superimposed on the scatterplots of the data for the UT variables velocity, attenuation, and RMS voltage in Fig. 4.

Velocity vs. AD.—For each RC level, the least squares quadratic curve rises to its apex and then falls (Fig. 4). The fall is more pronounced as RC increases, since velocity is sensitive to density changes caused by diminishing void volume as void spaces are ''filled up''; moreover, better bonding occurs at higher RC levels. Particularly in the RC 2% panels, the low value for the coefficient of determination ($R^2 = 0.46$ from Table 3) was due to high variability of the UT variable velocity caused by poor interfacial flake bonding in the panels. Comparing intersection points of the least squares curves across the RC levels (Table 3), the velocity RC 2% curve intersects the RC 4% (6%) curve at the AD values 0.35 and 1.13 (0.40 and 0.93). Note that both 0.35 and 1.13 are outside the observed data range, while 0.40 and 0.93 are both within. The velocity RC 4% curve intersects the RC 6% curve at the AD values 0.42 and 0.86, again, both values being within the observed data range. The velocity values corresponding to the AD values 0.42 and 0.86 are 0.67 km/s and 1.19 km/s, respectively. Clearly, maximum velocity occurs at RC 6% in combina-

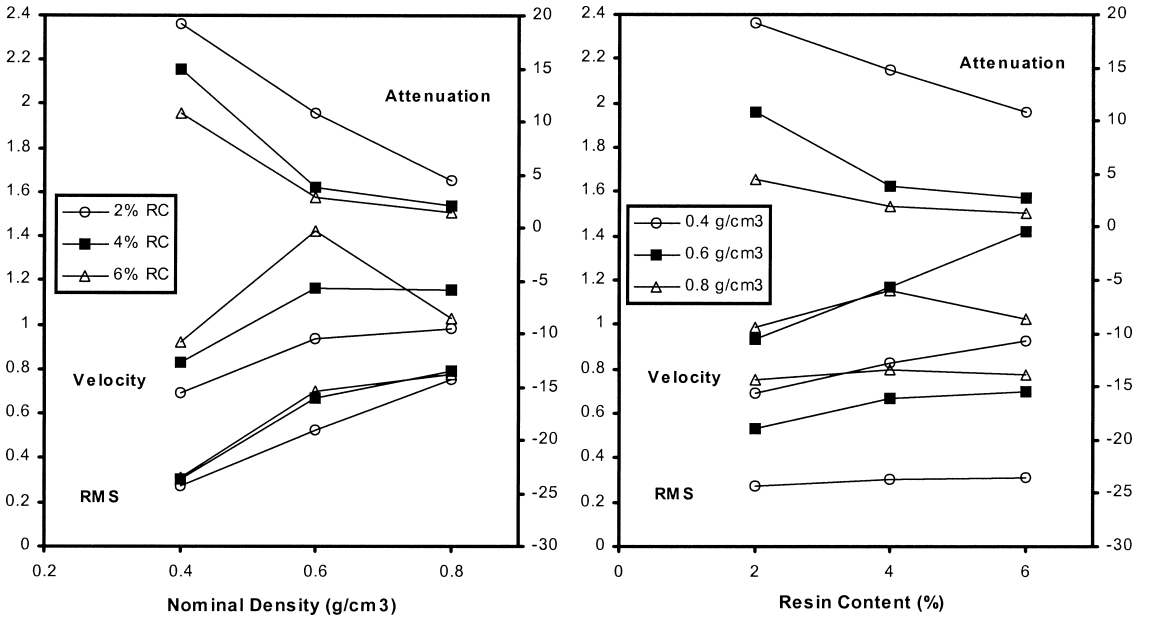

FIG. 3. Scatter plots for the group averages of UT variables velocity, attenuation, and RMS voltage as a function of nominal density (a) and resin content (b) levels.

tion with 0.6 ND. These suggest that velocity is subject to the physical integrity of the interfacial bonding between flakes.

Attenuation/RMS voltage vs. AD.—For each RC level, the least squares quadratic curve for attenuation decreases with increasing density, with only a slight increase for the RC levels 4% and 6% (Fig. 4). The least squares curves for the RMS voltage increase with increasing density, with only a slight decrease for RC 6% level. Comparing intersection points of the least squares curves across the RC levels (Table 3), the attenuation RC 2% curve intersects the RC 4% (6%) curve at the AD values 0.32 and 1.00 (-0.02 and 1.03). The attenuation values corresponding to the AD values 0.32 and 1.00 are 26.1 dB and 2.50 dB, respectively. The attenuation RC 4% curve does not intersect the RC 6% curve; instead, minimum attenuation occurs for both of these curves at the AD value of approximately 0.89 g/cm^3. The RMS voltage RC 2% curve intersects the RC 4% (6%) curve at the AD values 0.45 and 1.00 (0.44 and 0.94), while RC 4% intersects RC 6% curve at 0.43 and 0.82 g/cm^3. All these values are within the observed data range. In general, velocity and RMS voltage increase with increasing AD, whereas attenuation decreases with increasing AD. These facts also show that both attenuation and RMS voltage are invariant to interfacial boundary impediments, making them a reliable gauge to diagnose internal structure of materials.

Density prediction

A calibration procedure was developed to predict the AD from each of the UT measurements. For each RC level, the plot of AD versus the UT variables reveals a quadratic relationship (Fig. 5). Accordingly, a quadratic regression was performed for each of the nine data sets of Fig. 5. (Note that only data for ND 0.4 and 0.6 are plotted for the UT variable velocity at RC levels 4% and 6%). R^2 values for velocity increase with increasing RC levels, while R^2 values for RMS voltage are basically constant across RC levels. R^2 values

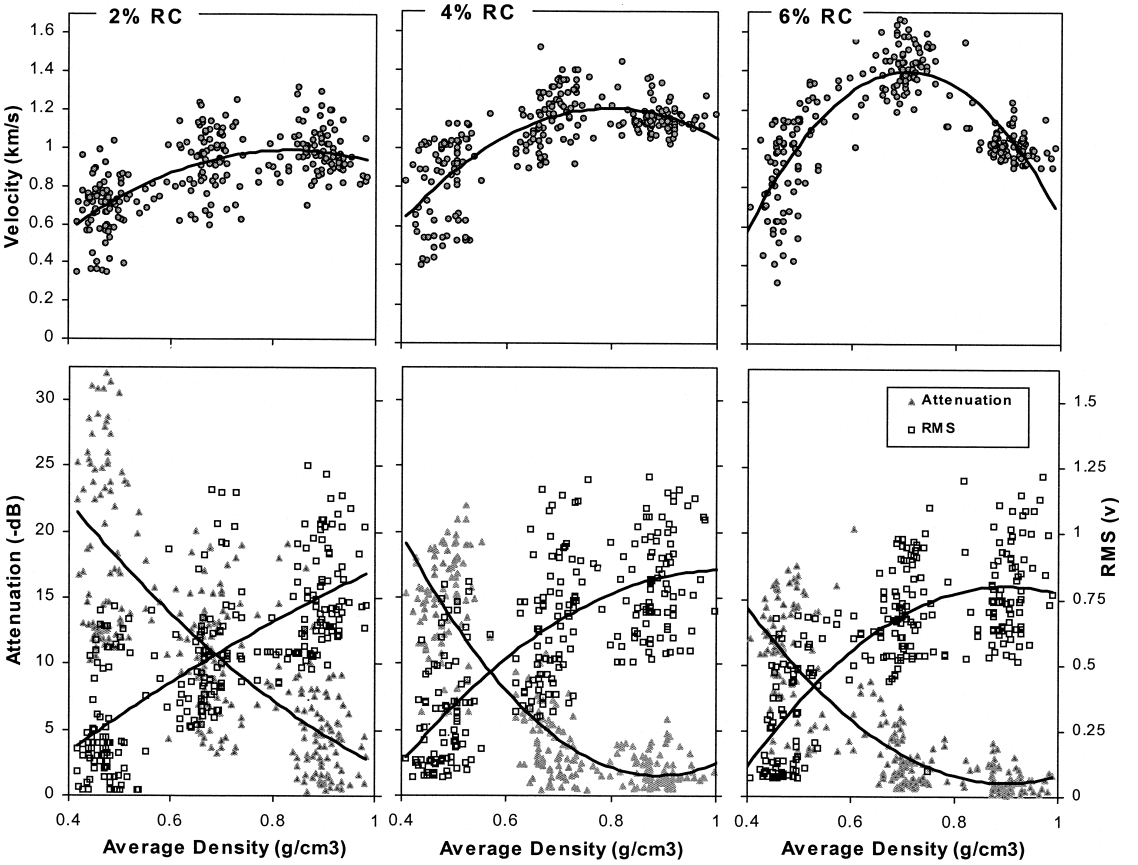

FIG. 4. Regressions of UT variables velocity, attenuation, and RMS voltage as a function of average density for boards at RC 2%, 4%, and 6% levels.

for attenuation increase as RC increases from 2% to 4%, and decrease slightly from RC 4% to 6%.

Percent out-of-limits (POFL) of the predicted values (i.e., the predicted values within a panel that are not within 10% of the average of the measured AD's for the panel) for these simple regression models were, in general, high (e.g., when the quadratic model for velocity was fit to all of the data, the out-of-limits predicted values for all RC and ND combinations exceeded 68%, the lone exception being RC 6% with ND 0.60). To improve on the POFL predicted values, logarithmic, power, and/or product functions of the original UT variables were included to form new models.

The general model having 18 predictors used for any given RC level is

$$Y_{ij} = B_0 + \sum_{k=1}^{3} A_k \,\mathrm{Ln}(X_{ijk}) + \sum_{k=1}^{3} C_k X_{ijk} + \sum_{k=1}^{3} D_k X_{ijk}^2 + \sum_{k=1}^{3} E_k \,\mathrm{Ln}(X_{ijk}) \cdot X_{ijk} + \sum_{k \neq k'} \sum F_k \,\mathrm{Ln}(X_{ijk}) \cdot X_{ijk'} + \varepsilon_{ij} \qquad (5)$$

where Y_{ij} is the AD measurement for specimen ij obtained from the grid i and j, X_{ijk} is the UT measurement (k = 1 velocity, k = 2 attenuation, k = 3 RMS voltage) for specimen ij, ϵ_{ij} is the random error term, B_o is the intercept, and A_k, C_k, D_k, E_k, F_k are the coefficients.

TABLE 3. *Least squares quadratic curves UT = $B_2(AD)^2 + B_1(AD) + B_0$ and points of intersection (by RC levels).*

UT variable	RC	B_2	B_1	B_0	R^2
		(a) Least Squares Curves Quadratic Function			
Velocity	2%	−2.24	3.74	−0.57	0.46
	4%	−3.71	5.91	−1.15	0.55
	6%	−8.69	12.27	−2.94	0.68
Attenuation	2%	23.12	−65.23	44.65	0.57
	4%	75.73	−134.9	61.59	0.77
	6%	53.20	−95.71	44.12	0.70
RMS Voltage	2%	−0.40	1.71	−0.46	0.51
	4%	−1.90	3.89	−1.13	0.55
	6%	−2.74	4.94	−1.42	0.61
		(b) AD points of Intersection of Least Squares Curves (corresponding UT values appear in brackets).*			
Velocity	2%		1.13[0.79]		0.93[0.97]
	0.35[0.47]		4%		0.86[1.19]
	0.40[0.56]		0.42[0.67]		6%
Attenuation	2%		0.32[26.1]		−0.02[45.8]
	1.00[2.50]		4%		##
	1.03[1.98]		##		6%
RMS Voltage	2%		1.00[0.86]		0.94[0.80]
	0.45[0.23]		4%		0.82[0.78]
	0.44[0.22]		0.43[0.19]		6%

* $AD = [-D_1 \pm (D_1{}^2 - 4D_2\ D_0)^{0.5}]/(2D_2)$ where $D_i = (B_{i,RC} - B_{i,RC'})$ with i = 0,1,2.
Attenuation RC 4% and 6% quadratics do not intersect; minimum attenuation occurs at AD value of approximately 0.89 for each.

An alternative polynomial model for the density, also with 18 predictors, for any given RC level is

$$Y_{ij} = B_0 + \sum_{k=1}^{3} A_k X_{ijk} + \sum_{k=1}^{3} C_k X_{ijk}^2 + \sum_{k=1}^{3} D_k X_{ijk}^3 + \sum_{k \neq k'} \sum E_k X_{ijk} \cdot X_{ijk'} + \sum_{k \neq k'} \sum F_k X_{ijk} \cdot X_{ijk'}^2 + \varepsilon_{ij} \quad (6)$$

For each of three data sets (Data 1 = ND 0.4, 0.6, 0.8, Data 2 = 0.4, 0.6 only, Data 3 = 0.6, 0.8 only), final models were obtained from the backward elimination procedure using least squares regression. Backward elimination starts with the full model and removes variables one at a time until all variables remaining are significant at 0.10 level. All of the final models obtained had significant variable coefficients. For example, all coefficients in the general model when applied to Data 3 for RC 4% are significant with $p \leq 0.0013$ (Table 4).

Judging from the standardized coefficient values, the velocity (RMS voltage and/or attenuation) terms contribute more profoundly to both the general and polynomial models for the higher density specimens of Data 3 at the higher (lower) RC levels (see Table 4 for the standardized coefficients of the general model). As is the case for Data 3, velocity and the RMS voltage/attenuation combination form complementary terms in influencing AD for Data 2. Again, this suggests that the velocity predictor is influenced by weak bonding or physical impediments in the interfacial boundaries; whereas, both the attenuation and RMS voltage predictors provide good indicators for ultrasonic energy transmissivity.

For both the general and polynomial final models, R^2 increases with increasing RC levels for Data 1 and Data 2. For Data 3, however, R^2 decreases from RC 2% to 4%, before increasing to its maximum value at RC 6%. For the same Data and RC levels, R^2 values for the general and polynomial final models are very similar (Table 5).

Predicted Residual Sum of Squares

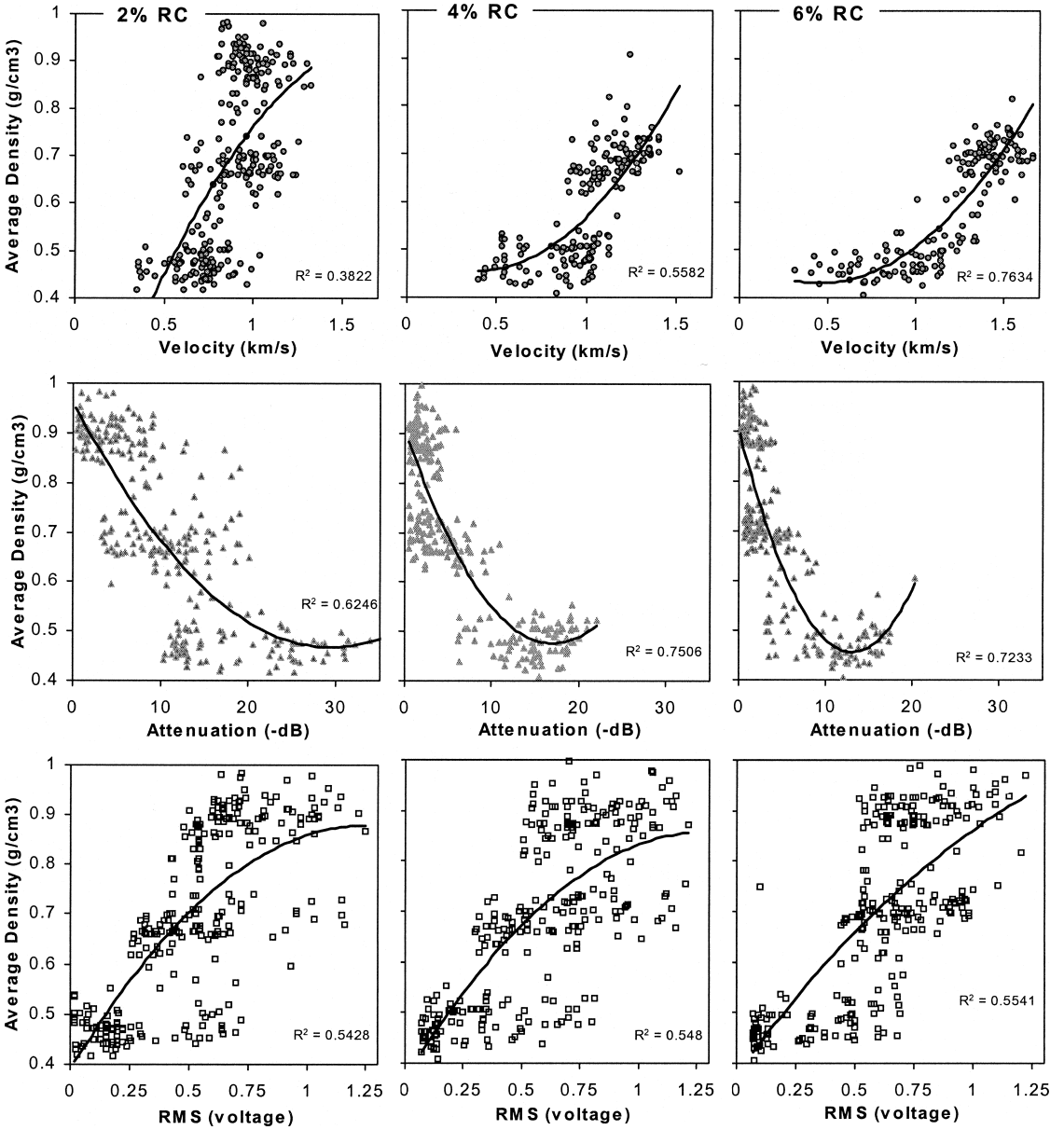

FIG. 5. Calibration regressions of measured density as a function of UT predictors velocity, attenuation, and RMS voltage for boards at RC 2%, 4%, and 6% levels.

(PRESS) was obtained for each of the final regression models. PRESS is calculated as Σd_i^2, where $d_i = Y_i - \hat{Y}_{i(i)}$ for $\hat{Y}_{i(i)}$ the predicted value for the *i*th observation using coefficient estimates obtained when the *i*th observation is deleted; d_i also equals $(Y_i - \hat{Y}_i)/(1 - h_{ii})$, when $\hat{Y}_i$ is the predicted value for the *i*th observation using all of the data, and h_{ii} is the *i*th diagonal element of the Hat matrix using all of the data (Neter et al. 1996).

Both the polynomial and general models exhibit a decreasing trend in square root PRESS as RC levels increase for Data 1. For Data 2, root PRESS decreases as RC increases from

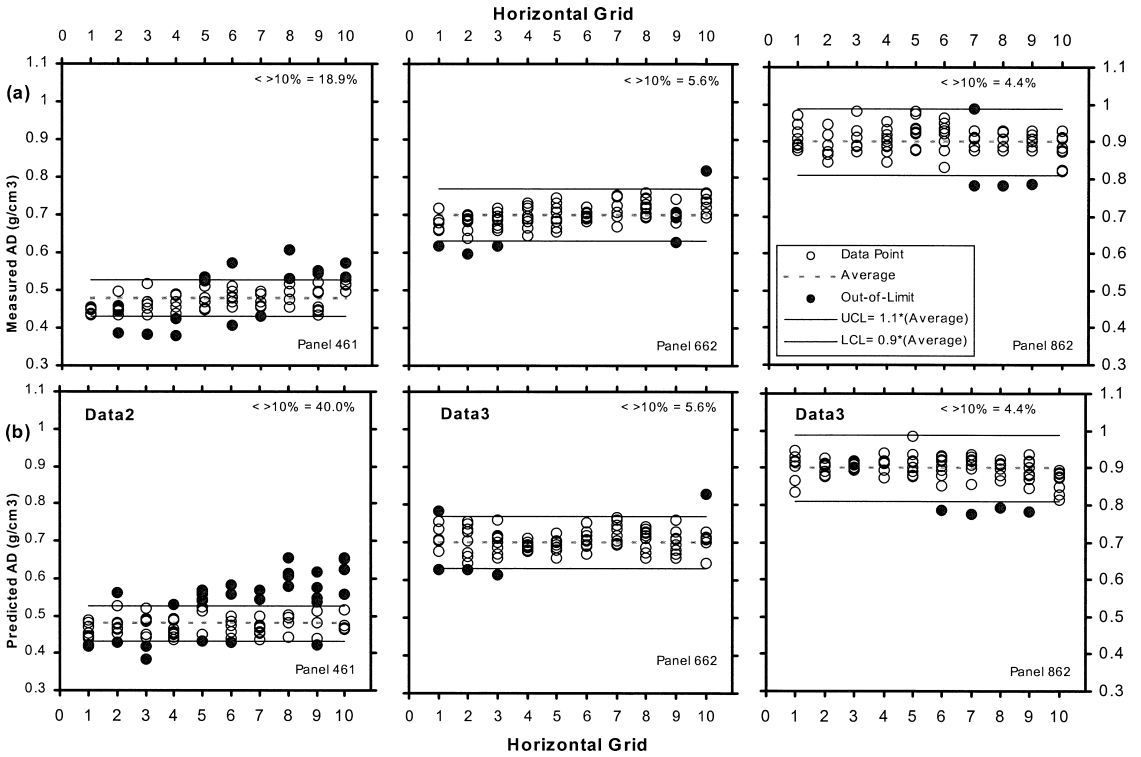

FIG. 6. Control charts for measured AD's (a) and predicted polynomial AD's (b) for the ND 0.40, 0.60, 0.80 RC 6% panels.

2% to 4% and then remains basically constant as RC increases from 4% to 6%. For Data 3, root PRESS increases and then drops to its minimum value as RC levels increase (Table 5). Trends also exist in the R^2 values as RC increases. These trends are more complementary (as opposed to similar) in nature to the root PRESS trends.

Average density validation

The EN300 panel standard allows for a 10% variation from the average of the measured AD's within a panel. Accordingly, the control lower (upper) limit for a panel is 0.90·panel average measured AD's (1.10·panel average measured AD's). Control limits for the measured AD's were evaluated for each of the nine panels included in this study (see Table 5). Note that for the ND 0.40 panels, POFL increased as RC increased, all three POFL's exceeding the allowed 10%. For the ND 0.60 panels, POFL decreased as RC increased, with only the RC 2% panel marginally out-of-limits (10%). For the ND 0.80 panels, all RC levels had POFL less than 10%. Using our nine sets of control limits, it appears necessary to manufacture at least 0.60 g/cm^3 panels to conform to the EN300 standard.

For all final models, the predicted AD's were *in situ* matched with the measured AD's for each test panel. The POFL for the predicted values in each panel using the EN300 panel control limits was computed for each model and is reported in Table 5 for each data set. Generally, the models for Data 1 produce greater overall prediction error than those for Data 2 or Data 3 (the root PRESS values exhibit the same tendencies). For the polynomial model using Data 1, the smallest POFL was 17.8%, attained at both RC 4% ND 0.80 and RC 6% ND 0.60. Generally using Data 1, predictions at the RC 2% level did not agree with

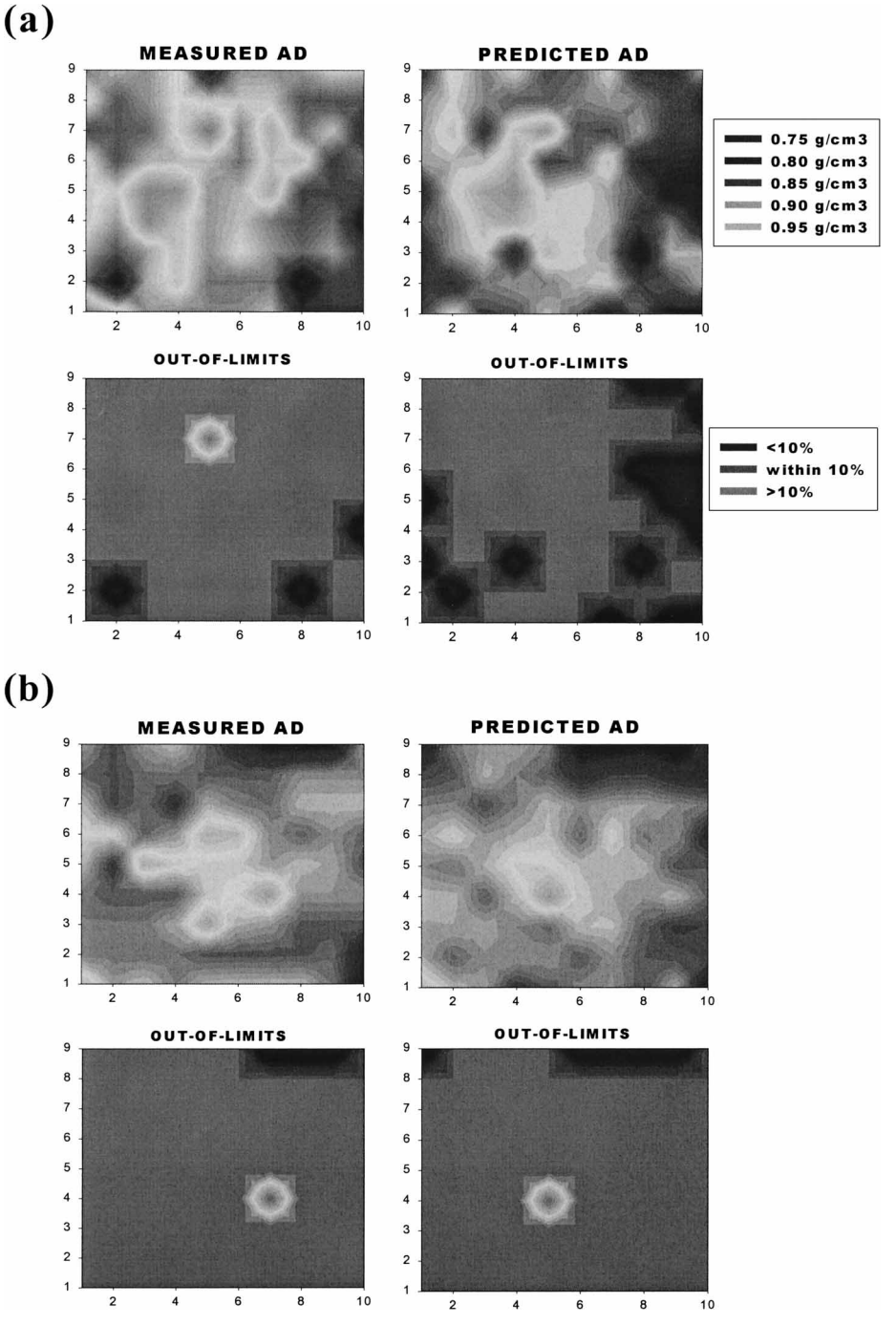

FIG. 7. Contour spatial distribution and out-of-limits plots comparing the measured and predicted general AD's for RC 2% (a) and RC 6% (b) both at ND 0.80 g/cm^3 applied in Data 3.

TABLE 4. *General and Polynomial Models for predicting density (AD) as a function of the UT variables: V, A, R = Velocity (km/s), Attenuation (−dB), RMS Voltage (v) for Data3.*

	General Model: AD = B_0 + Ln(V) + Ln(A) + Ln(R) + V + A + R + V^2 + A^2 + R^2 + Ln(V)*V + Ln(V)*A + Ln(V)*R + Ln(A)*V + Ln(A)*A + Ln(A)*R + Ln(R)*V + Ln(R)*A + Ln(R)*R					*Polynomial Model:* AD = B_0 + V + V^2 + V^3 + A + A^2 + A^3 + R + R^2 + R^3 + VA + VR + AR + V^2A + VA^2 + V^2R + VR^2 + A^2R + AR^2				
RC	Variable	Est.	StdErr	Pr>|t|	Std Est.	Variable	Est.	Std.Err	Pr>|t|	Std. Est.
2%	B_0	−28.70	7.65	0.0002	0.0	B_0	−0.10	0.12	0.4171	0.0
	Ln(V)	−1.09	0.37	0.004	−1.4	A^2	0.00	0.00	0.0835	−0.6
	Ln(R)	−8.97	2.47	0.0004	−29.6	R	4.97	0.80	<.0001	10.2
	R	16.00	4.32	0.0003	32.8	R^2	−3.77	0.84	<.0001	−11.1
	V^2	0.42	0.16	0.0111	1.0	VR	−2.39	1.06	0.0258	−5.7
	R^2	13.19	3.49	0.0002	38.7	AR	−0.05	0.01	<.0001	−0.9
	Ln(V)*A	0.08	0.02	<.0001	1.3	R^3	1.24	0.38	0.0012	4.4
	Ln(A)*V	−0.27	0.09	0.0021	−1.9	VA^2	0.00	0.00	0.0007	1.1
	Ln(A)*R	0.15	0.09	0.0928	0.6	V^2R	0.99	0.51	0.0526	2.8
	Ln(R)*A	−0.03	0.01	0.0006	−1.3					
	Ln(R)*R	−33.97	8.60	0.0001	−44.2					
4%	B_0	−37.46	6.68	<.0001	0.0	B_0	−8.56	3.40	0.0128	0.0
	Ln(A)	−3.29	0.54	<.0001	−22.8	V	29.68	8.60	0.0007	30.7
	A	0.36	0.08	<.0001	7.0	V^2	−24.26	7.28	0.0011	−59.0
	V^2	20.37	5.02	<.0001	49.6	A	−1.01	0.21	<.0001	−19.8
	A^2	−0.02	0.01	0.0003	−3.6	A^2	0.10	0.02	<.0001	18.6
	R^2	17.44	2.66	<.0001	54.8	R	−3.43	0.67	<.0001	−7.2
	Ln(V)*V	−47.48	10.99	<.0001	−56.8	AR	1.17	0.29	<.0001	9.2
	Ln(V)*A	−0.35	0.10	0.0008	−1.3	V^3	6.51	2.04	0.0017	28.4
	Ln(V)*R	8.81	1.44	<.0001	6.6	A^3	0.00	0.00	0.0003	−5.5
	Ln(A)*V	0.96	0.29	0.0013	7.4	R^3	0.94	0.20	<.0001	3.6
	Ln(A)*R	1.85	0.27	<.0001	7.6	A^2R	−0.06	0.02	0.0005	−5.0
	Ln(R)*V	−4.46	0.58	<.0001	−15.3	AR^2	−0.28	0.11	0.0115	−1.4
	Ln(R)*A	−0.18	0.05	0.0007	−3.6					
	Ln(R)*R	−31.03	4.82	<.0001	−44.6					
6%	B_0	388.21	124.30	0.0021	0.0	B_0	−2.72	0.71	0.0002	0.0
	Ln(V)	174.81	54.00	0.0015	293.3	V	9.79	1.72	<.0001	20.1
	Ln(A)	0.16	0.07	0.0248	1.3	V^2	−7.75	1.38	<.0001	−39.6
	Ln(R)	−0.62	0.15	.0001	−1.6	A	0.25	0.11	0.0289	4.0
	V	−342.43	106.66	0.0016	−701.6	A^2	0.01	0.00	0.0045	1.7
	V^2	−48.49	17.83	0.0072	−247.7	VA	−0.68	0.16	<.0001	−15.5
	R^2	3.67	0.75	<.0001	9.6	VR	−0.99	0.19	<.0001	−2.5
	Ln(V)*V	264.13	88.30	0.0032	655.8	AR	0.21	0.05	<.0001	1.9
	Ln(V)*A	0.16	0.04	<.0001	1.0	V^3	1.89	0.36	<.0001	18.4
	Ln(A)*V	−0.23	0.06	0.0002	−2.3	R^3	0.22	0.04	<.0001	0.7
	Ln(A)*A	−0.02	0.00	<.0001	−0.7	V^2A	0.29	0.06	<.0001	9.5
	Ln(A)*R	0.13	0.03	<.0001	0.7	V^2R	0.45	0.10	<.0001	2.1
	Ln(R)*V	−0.23	0.10	0.0202	−0.8	A^2R	−0.02	0.01	0.0033	−1.7
	Ln(R)*R		1.29	<.0001	−7.5					

their measured counterparts, producing POFL's ≥ 31.1%.

For the general model applied to Data 2, the minimum POFL of 11.1% was attained at both RC 4% ND 0.40 and RC 6% ND 0.60. For the polynomial model applied to Data 2, the minimum POFL of 8.9% was attained at RC 4% and ND 0.60. When restricted to Data 3, both the general and polynomial models were within the 10% control limits for RC 6%. This suggests that the models required at least 0.60 g/cm^3 targeted nominal density for ultrasonic monitoring of OSB horizontal density variation.

The dispersion of the predicted out-of-limits points was similar to the spatial dispersion of the measured out-of-limits points, as is seen in

TABLE 5. *Summary of out-of-limits percentages for AD measured and predicted values.*

Test panels			Control limits ±10%	Out-of-Limits <>10% density variation						
					General model			Polynomial model		
RC (%)	ND (g/cm^3)	AD (g/cm^3)		Measured data	Data1	Data2	Data3	Data1	Data2	Data3
2%	0.40	0.476	[.429, .524]	12.2%	46.7%	53.3%		51.5%	52.2%	
	0.60	0.686	[.618, .755]	10.0%	35.6%	28.9%	36.7%	34.4%	27.8%	44.4%
	0.80	0.894	[.805, .984]	4.4%	33.3%		18.9%	31.1%		24.4%
				R^2	0.72	0.56	0.64	0.74	0.58	0.60
				√PRESS	(1.58)	(1.09)	(0.96)	(1.54)	(1.06)	(1.00)
4%	0.40	0.482	[.435, .531]	14.4%	24.4%	11.1%		18.9%	13.3%	
	0.60	0.691	[.622, .760]	8.9%	43.3%	12.2%	40.0%	51.1%	8.9%	46.7%
	0.80	0.887	[.798, .976]	7.8%	20.0%		18.9%	17.8%		16.7%
				R^2	0.83	0.83	0.56	0.81	0.82	0.49
				√PRESS	(1.23)	(0.63)	(1.09)	(1.27)	(0.65)	(1.27)
6%	0.40	0.479	[.432, .527]	18.9%	44.4%	41.1%		47.8%	40.0%	
	0.60	0.699	[.629, .769]	5.6%	21.1%	11.1%	3.3%	17.8%	12.2%	5.6%
	0.80	0.899	[.810, .989]	4.4%	24.4%		6.7%	21.1%		4.4%
				R^2	0.86	0.84	0.91	0.86	0.85	0.90
				√PRESS	(1.15)	(0.67)	(0.57)	(1.15)	(0.65)	(0.47)

Notes: Control Limits: within 10% deviation from individual measured AD's obtained from each test panel.
Out-of-limits: percent of 90 specimens not within Control Limits.
Data1: fit to ND's 0.4, 0.6, and 0.8 (270 specimens total).
Data2: fit to ND's 0.4 and 0.6 only (180 specimens total).
Data3: fit to ND's 0.6 and 0.8 only (180 specimens total).

Fig. 6. In as much as we want to replicate the natural fluctuation of the density variations, the smoothing effects of the regressions result in some discrepancies in the *in situ* locations of the predicted AD's. Fig. 7 compares a typical spatial color contour of the measured to predicted AD's in the RC 2% and 6% panels. There is a reasonable spatial resemblance of the horizontal density to the measured AD's as predicted by the general models. The general models are spatially cohesive to the measured AD's, shown by the out-of-limits points (the polynomial models are not especially cohesive). Again, by visual comparisons, the prediction of the density improves with increasing ND and RC levels.

Sampling effects of this contact ultrasonic technique may contribute to the AD measurement errors. For example, the corners of the 51×51-mm^2 IB specimen (contributing to the additional density measure) are not accounted for in the ultrasonic readings as limited by the circular transducer size. Smaller transducers may provide different resolution (i.e., sampling size) to capture the representative material characteristics (determined by flake dimension, resin content and distribution, and prevalence of fines and/or macrovoids) that are contained within the specimen. Optimal sampling size for capturing ultrasonic information remains unknown.

CONCLUSIONS AND RECOMMENDATIONS

Horizontal density variation is inherent in OSB, because of random particle deposition in the mat formation process resulting in inevitable voids (of low-density range) and discrete consolidated particle structure (of high-density range). Having consistent horizontal density distribution within a flakeboard is important in determining its creep resistance and durability in service.

Ultrasonic nondestructive techniques provide valuable tools in product design and property characterizing and monitoring. Mechanical properties of OSB can be approximated using the UT variable responses. Particularly, velocity is sensitive to density changes caused by the mechano-chemical process of panel densification in the hot press. As mentioned earlier, the attenuation vs. AD qua-

dratic curves for RC 4% and 6% intersect at the AD value 0.89 g/cm^3 (Table 3), which marks the transitional density separating the stage of diminishing void volume (at low density) and the stage of increasing plastic-strain hardening (at high density). This transitional density of 0.89 g/cm^3 is in close agreement with that of 0.90 g/cm^3 for aspen OSB found by Vun et al. (2003).

For the low RC and ND levels, the existence of high variability in the UT responses also corresponds to high variability in the measured average density, attributed to the existence of within-panel low-density elements and discontinuities arising from poor interfacial flake bonding zones. As discussed earlier, velocity is an influential predictor of AD when nominal density exceeds 0.60 g/cm^3. An influential velocity variable coincides with higher density (i.e., fewer voids and therefore, less physical impediment in the propagation path); whereas, influential attenuation and RMS voltage variables coincide with a high level of ultrasonic energy transmission through a low density medium. The different responses of the UT variables to density across the RC and ND levels, therefore, form excellent complementary predictors of density.

UT investigation of the horizontal density is convenient and appropriate for monitoring structural quality of a large panel. This study acknowledges the challenging problems in wood composite studies that can cause grossly attenuated UT signal responses due to coupling contact systems, board surface quality, panel anisotropy, properties of wood flakes, and presence of interfacial macrovoids between flakes. UT responses may also be adversely affected by the composition of the medium, as well as the transducer size (and the corresponding sampling area). We recommend further studies (1) to explore other orthoregression, partial least squares, nonlinear and geostatistic approaches to spatial modeling, (2) to explore other coupling systems, and (3) to investigate the effects of sampling/transducer size on the density and ultrasonic measurements.

ACKNOWLEDGMENT

The financial support to this project by USDA NRI Competitive Grant Program (99-351103-8298) is gratefully acknowledged.

REFERENCES

BEALL, C. F. 2002. Overview of the use of ultrasonic technologies in research on wood properties. Wood Sci. Technol. (36):197–212.

BUCUR, V., M. P. ANSELL, C. Y. BARLOW, J. PRITCHARD, S. GARROS, AND X. DEGLISE, 1998. Physical methods for characterizing wood composite. Holzforschung (52): 553–561.

CHEN, L-H, AND F. C. BEALL. 2000. Monitoring bond strength development in particleboard during pressing, using acousto-ultrasonics. Wood Fiber Sci. 32(4):466–477.

KRUSE, K., C. DAI, AND A. PIELASCH. 2000. An analysis of strand and horizontal density distributions in oriented strand board. Holz Roh-Werkst. 58(4):270–277.

JEONG, H., AND D. K. HSU. 1995. Experimental analysis of porosity-induced ultrasonic attenuation and velocity change in carbon composites. Ultrasonics 33(3):195–203.

JUDD, N. C. W., AND W. W. WRIGHT. 1978. Voids and their effects on the mechanical properties of composites—An appraisal. SAMPE Journal, January/February: 10–14.

LENTH, C. A., AND F. A. KAMKE. 1996. Investigations of flakeboard mat consolidation. Part I. Characterization the cellular structure. Wood Fiber Sci. 28(2):153–167.

LU, C., AND F. LAM. 2001. Random field representation of horizontal density distribution: I. Partially oriented strandboard mat. Wood Fiber Sci. 33(3):437–449.

NETER, J., M. H. KUTNER, C. J. NACHTSHEIM, AND W. WASSERMAN. 1996. Applied linear statistical models. 4th Ed. Irwin McGraw-Hill, Chicago, IL. pp. 345–373.

OUDJEHANE, A., AND F. LAM. 1998. On the density profile within random and oriented wood-based composite panels: Horizontal distribution. Composites Part B 29B: 687–694.

ROSS, R. J., AND R. F. PELLERIN. 1988. NDE of wood-based composites with longitudinal stress waves. Forest Prod. J. 38(5):38–45.

SMITH, C. D. 1982. Waferboard press closing strategies. Forest Prod. J. 32(3):40–45.

STEINER, P. R., AND C. DAI. 1993. Spatial structure of wood composites in relation to processing and performance characteristics: Part 1. Rationale for model development. Wood Sci. Technol. (28):45–51.

SUCHSLAND, O. 1962. The density distribution in flakeboard. Q. Bull., Michigan Agric. Exp. Sta., Michigan State Univ. 45(1):104–121.

———, AND H. XU. 1989. A simulation of the horizontal density distribution in a flakeboard. Forest Prod. J. 39(5):29–33.

SUDDARTH, S. K. 1965. Detection of adhesive bond defects

in the Polaris missile nose firing through mechanical impedance measurements. Pages 267–285 *in* 2nd Nondestructive Testing of Wood Symposium 1965. April, Washington State University, Pullman, WA.

VOGT, J. J. 1986. Longitudinal stress waves as predictors of internal bonding strength. 12th Particleboard/Composite Materials Symposium, March, 1985. Washington State University, WA.

VUN, R.Y-H, AND F. C. BEALL. 2002. Monitoring creep rupture in oriented strandboard using acoustic emission. *In* International NDT2002 Symposium, 19–21 August, 2002. University of California, Berkeley, CA.

——, Q. WU, M. C. BHARDWAJ, AND G. STEAD. 2003. Ultrasonic characterization of structural properties of oriented strandboard: Direct-contact vs. non-contact methods. Wood Fiber Sci. (in press). 35(2):——.